FULL PAPER

An Analytical Model of Reactive Diffusion for Transient Electronics

Rui Li, Huanyu Cheng, Yewang Su, Suk-Won Hwang, Lan Yin, Hu Tao, Mark A. Brenckle, Dae-Hyeong Kim, Fiorenzo G. Omenetto, John A. Rogers, and Yonggang Huang**

Transient electronics is a class of technology that involves components which physically disappear, in whole or in part, at prescribed rates and at programmed times. Enabled devices include medical monitors that fully resorb when implanted into the human body ("bio-resorbable") to avoid long-term adverse effects, or environmental monitors that dissolve when exposed to water ("eco-resorbable") to eliminate the need for collection and recovery. Analytical models for dissolution of the constituent materials represent important design tools for transient electronic systems that are configured to disappear in water or biofluids. Here, solutions for reactive-diffusion are presented in single- and double-layered structures, in which the remaining thicknesses and electrical resistances are obtained analytically. The dissolution time and rate are defined in terms of the reaction constants and diffusivities of the materials, the thicknesses of the layer, and other properties of materials and solution. These models agree well with the experiments for single layers of Mg and SiO_2, and double layers of Mg/MgO. The underlying physical constants extracted from analysis fall within a broad range previously reported in other studies; these constants can be extremely sensitive to the morphologies of the materials, temperature, and the PH value, concentration, and properties of the surrounding liquid.

1. Introduction

Typically, the development of an electronic system involves efforts to optimize the time duration of stable performance of the constituent devices, i.e., their physical and functional lifetimes. The materials and design layouts must be engineered carefully to meet this goal. A different kind of technology, referred to as transient electronics,[1] has, as a key characteristic, an opposite feature: it physically disappears at prescribed rates in a benign way when exposed, for example, to water in the environment or the body. Devices built in this manner create application opportunities that lie outside those that can be addressed using established classes of integrated circuits. Examples include medical monitors, interventional components or therapeutic vehicles that fully resorb when implanted into the human body ("bio-resorbable") to avoid long-term adverse effects. Others involve environmental monitors/sensors that dissolve when exposed to water ("eco-resorbable") to eliminate the need for collection and recovery.

The approaches reported by Hwang et al.[1] create foundations for a silicon based transient technology that can offer excellent performance, in a manner that leverages much of the scientific knowledge and engineering capabilities that have emerged from decades of fundamental and applied work on traditional forms of silicon electronics. When taken together with

Dr. R. Li
State Key Laboratory of Structural Analysis for Industrial Equipment
Department of Engineering Mechanics
Dalian University of Technology
Dalian 116024, China
Dr. R. Li, H. Cheng, Dr. Y. Su, Prof. Y. Huang
Department of Mechanical Engineering
Department of Civil and Environmental Engineering
Northwestern University
Evanston, IL 60208, USA
E-mail: y-huang@northwestern.edu
Dr. Y. Su
Center for Mechanics and Materials
Tsinghua University
Beijing 100084, China
S.-W. Hwang, Dr. L. Yin, Prof. J. A. Rogers
Department of Materials Science and Engineering
Beckman Institute for Advanced Science and Technology, Frederick Seitz Materials Research Laboratory, University of Illinois at Urbana-Champaign
Urbana, IL 61801, USA
E-mail: jrogers@illinois.edu
Dr. H. Tao, M. A. Brenckle, Prof. F. G. Omenetto
Department of Biomedical Engineering
Tufts University
Medford, MA 02155, USA
Prof. D.-H. Kim
School of Chemical and Biological Engineering
Institute of Chemical Processes
Seoul National University
Seoul 151-741, Republic of Korea

DOI: 10.1002/adfm.201203088

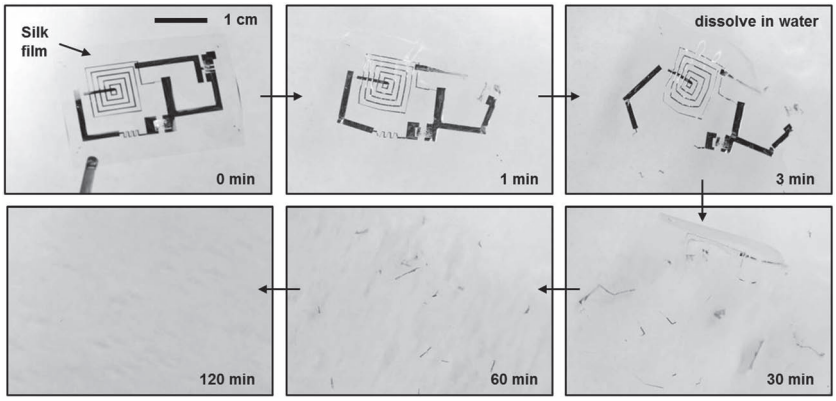

Figure 1. Image of a transient electronic system that includes all the essential components. All of the materials, silicon nanomembrane (semiconductor), thin film of magnesium (conductor), magnesium dioxide (dielectric and encapsulation layer), silicon dioxide (dielectric) and silk (substrate and overcoat material), are biocompatible in a sense that they will resorb by the body through hydrolysis or dissolution.

sensors, actuators, power supply and wireless control, this technology can exploit many modern, established aspects of device and circuit design, with access to capabilities that qualitatively exceed those available with recently reported forms of organic electronics in which only certain materials are transient[2–4] or of non-transient circuits that are formed on dissolvable substrates.[5]

Figure 1 shows a demonstration system that includes transient inductors, capacitors, resistors, transistors, diodes and interconnects, on a water soluble substrate. This example exploits silicon nanomembrane (Si NM) for semiconductors, magnesium (Mg) for the conductors, magnesium oxide (MgO) and silicon dioxide (SiO_2) for the dielectrics, and silk for the substrate and packaging materials. The solubility and rates of hydrolysis for silicon are exceptionally small; the NM is essential to minimize the total amount of silicon that much be consumed during the transient step. The dissolution of silicon in PBS (pH = 7.4, to match physiological levels) proceeds to yield silicic acid $Si(OH)_4$ following the equilibrium: $Si+4H_2O \leftrightarrow Si(OH)_4+2H_2$, where the dissolution sometimes involves the oxidation to SiO_2 as an intermediate product. The kinetics can be simply captured by considering a constant reaction rate at Si surface, and this surface reaction model agrees with the experimental measurements at both body and room temperatures.[1]

Surface reaction may be enough to account for the dissolution of materials in crystalline structure as in Si[6] or other chemical reactions with large reaction constants, such as oxidation of magnesium,[7] corrosion of iron[8] and burning of wood.[9] However, diffusion becomes important for porous materials such as Mg, MgO deposited by electron beam evaporation, and SiO_2 deposited by plasma enhanced chemical vapor deposition, as shown in Figure 1. Here, the kinetics in alkaline solutions is described analytically using models of reactive diffusion[10] in which the rate limiting step is defined by diffusion of water and hydroxide ions into the porous material and reaction throughout the thickness direction.

This paper applies the reactive diffusion model[10] to the transient electronic systems. An analytical solution of the remaining height of the material is given, which in turn gives the resistance (per unit length) of Mg conductors. The results are compared with experiments, and the validated analytical model not only provides important insights of the transient behavior of the device, but is also useful as design guidelines.

In transient electronic systems, a period of stable operation defined typically by dissolution of the encapsulation layers is followed by functional degradation in a narrow time interval defined by dissolution of electrode itself. First, we introduce a single-layer reactive diffusion model in Section 2 for dissolution of porous materials, such as Mg (as electrodes) or SiO_2 (as dielectrics). A double-layer reactive diffusion model is established in Section 3 for the double-layer structure where the encapsulation layer (MgO) is on top of the porous material (Mg).

2. Single-Layer Reactive Diffusion

The process begins when a layer of porous material (e.g., Mg or SiO_2) is submerged in water (or PBS solution). The initial layer thickness h_0 is much smaller than the layer width/length such that the one-dimensional reactive diffusion model can be applied in the thickness direction y (**Figure 2**a), with $y = 0$ at the bottom of the layer. The reactive diffusion equation is[10]

$$D\frac{\partial^2 w}{\partial y^2} - kw = \frac{\partial w}{\partial t}, \quad 0 \le y \le h_0 \tag{1}$$

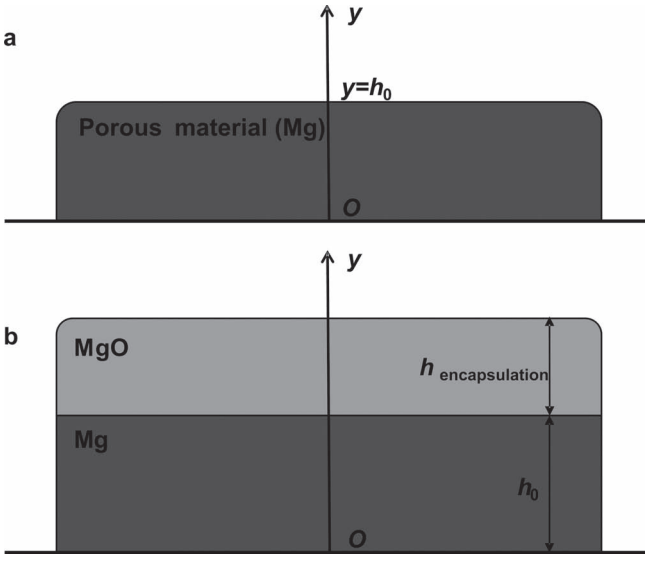

Figure 2. Schematic illustration of analytical models for reactive diffusion in hydrolysis; a) single layered structure; and b) double layered structure.

where D and k are the diffusivity of water and reaction constant between the porous material and water, respectively, w is the water concentration that depends on position y and time t. The above equation degenerates to the standard diffusion equation when the reaction term kw is neglected. For 5 mol% Fe-activated Mg, the reaction constant k ranges from 0.2×10^{-3} to 3×10^{-3} s^{-1},[11] depending on the chloride ion concentration from 0 to 5 M in water. Besides ion concentration, k also depends on many other factors such as the morphologies of the materials, temperature, and the PH value, concentration, and properties of the surrounding liquid.

Water concentration is constant w_0 at the interface between water and porous material whereas the water flux at the bottom surface of the porous material layer is zero, i.e.,

$$w|_{y=h_0} = w_0$$
$$\left.\frac{\partial w}{\partial y}\right|_{y=0} = 0 \tag{2a,b}$$

The initial condition is zero water concentration, i.e.,

$$w|_{t=0} = 0 \quad (0 \le y < h_0) \tag{3}$$

For the new variable $\theta = w - w_0$, Equation (1) – Equation (3) become

$$D\frac{\partial^2 \theta}{\partial y^2} - k\theta - \frac{\partial \theta}{\partial t} = kw_0, \quad 0 \le y \le h_0 \tag{4}$$

$$\theta|_{y=h_0} = 0$$
$$\left.\frac{\partial \theta}{\partial y}\right|_{y=0} = 0 \tag{5a,b}$$

$$\theta|_{t=0} = -w_0 \quad (0 \le y < h_0) \tag{6}$$

The homogeneous solution θ_h of Equation (4), $D\partial^2\theta_h/\partial y^2 - k\theta_h - \partial\theta_h/\partial t = 0$, and homogeneous boundary conditions $\theta_h|_{y=h_0} = 0$ and $\partial\theta_h/\partial y|_{y=0} = 0$ from Equation (5) can be solved by the method of separation of variables

$$\theta_h = Y(y)\,T(t) \tag{7}$$

This gives

$$D\frac{Y''}{Y} - k = \frac{T'}{T} = -\lambda \tag{8}$$

where λ is the eigenvalue to be determined. The solution of Equation (8) is

$$Y = A\sin\left(\sqrt{\frac{\lambda - k}{D}}y\right) + B\cos\left(\sqrt{\frac{\lambda - k}{D}}y\right)$$
$$T = e^{-\lambda t} \tag{9a,b}$$

where A and B are constants to be determined. The homogeneous boundary conditions become $Y|_{y=h_0} = 0$ and $Y'|_{y=0} = 0$, which give $A = 0$ and

$$\cos\left(\sqrt{\frac{\lambda - k}{D}}h_0\right) = 0 \tag{10}$$

Its solution gives the eigenvalues

$$\lambda_n = \left(\frac{2n-1}{2h_0}\pi\right)^2 D + k \quad (n = 1, 2, 3, \cdots) \tag{11}$$

The homogeneous solution is

$$\theta_h = \sum_{n=1}^{\infty}\left\{B_n e^{-\left[\left(\frac{2n-1}{2h_0}\pi\right)^2 D + k\right]t}\cos\left(\frac{2n-1}{2h_0}\pi y\right)\right\} \tag{12}$$

where the constants B_n are to be determined.

The general solution of Equation (4) is the sum of homogeneous solution in Equation (12) and a particular solution,

$$\theta = \sum_{n=1}^{\infty}\left\{B_n e^{-\left[\left(\frac{2n-1}{2h_0}\pi\right)^2 D + k\right]t}\cos\left(\frac{2n-1}{2h_0}\pi y\right)\right\} + w_0\left[\frac{\cosh\left(\sqrt{\frac{k}{D}}y\right)}{\cosh\left(\sqrt{\frac{k}{D}}h_0\right)} - 1\right] \tag{13}$$

where the last term is a particular solution that satisfies Equation (4) and Equation (5). Substitution of Equation (13) into the initial condition in Equation (6) gives

$$B_n = \frac{4(-1)^n(2n-1)\pi D w_0}{4kh_0^2 + (2n-1)^2\pi^2 D} \tag{14}$$

These give the solution of Equation (1) as

$$w(y,t) = w_0\left\{\frac{\cosh\left(\sqrt{\frac{kh_0^2}{D}}\frac{y}{h_0}\right)}{\cosh\sqrt{\frac{kh_0^2}{D}}} + 2\sum_{n=1}^{\infty}\frac{(-1)^n\left(n-\frac{1}{2}\right)\pi}{\frac{kh_0^2}{D} + \left(n-\frac{1}{2}\right)^2\pi^2}e^{-\left[\frac{kh_0^2}{D} + \left(n-\frac{1}{2}\right)^2\pi^2\right]\frac{Dt}{h_0^2}}\cos\left[\left(n-\frac{1}{2}\right)\pi\frac{y}{h_0}\right]\right\} \tag{15}$$

It clearly shows the scaling law that the normalized water concentration, w/w_0, depends on the normalized position y/h_0, normalized time Dt/h_0^2 that scales with the diffusivity D, and a single non-dimensional parameter kh_0^2/D that scales with the ratio of reaction constant k to diffusivity D, i.e.,

$$\frac{w}{w_0} = \bar{w}\left(\frac{y}{h_0}, \frac{Dt}{h_0^2}, \frac{kh_0^2}{D}\right) \tag{16}$$

where $\bar{w}$ is a non-dimensional function obtained from Equation (15). For $kh_0^2/D = 0.18$, which corresponds to $k = 1.2 \times 10^{-3}$ s^{-1} that falls within the range of reaction constants reported by Taub et al.,[11] $D = 6.0 \times 10^{-12}$ cm^2 s^{-1}, and $h_0 = 300$ nm of Mg in the experiment, **Figure 3** shows the distribution of water concentration for the normalized time $Dt/h_0^2 = 0.1$, 0.2, 0.4, 0.8, 2 and ∞, where $Dt/h_0^2 = \infty$ corresponds to the steady-state limit

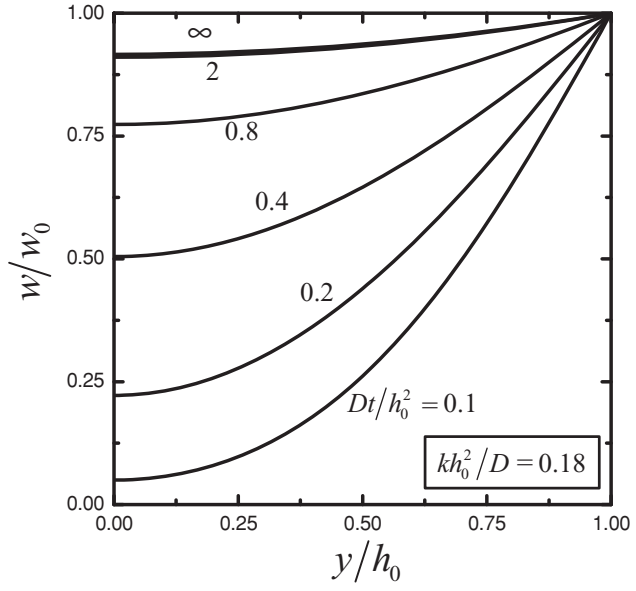

Figure 3. Distribution of water concentration in the Mg layer.

$$w(y, t \to \infty) = w_0 \frac{\cosh\left(\sqrt{\frac{kh_0^2}{D}}\frac{y}{h_0}\right)}{\cosh\sqrt{\frac{kh_0^2}{D}}} \tag{17}$$

which is effectively attained at finite time $Dt/h_0^2 = 2$. **Figure 4** shows the water concentration versus time at the middle ($y = h_0/2$) and bottom ($y = 0$) of the layer. It confirms that the steady-state limit is reached at $Dt/h_0^2 = 2$.

Let q denote the number of water molecules that react with each atom of the porous material. Since kw gives the mass

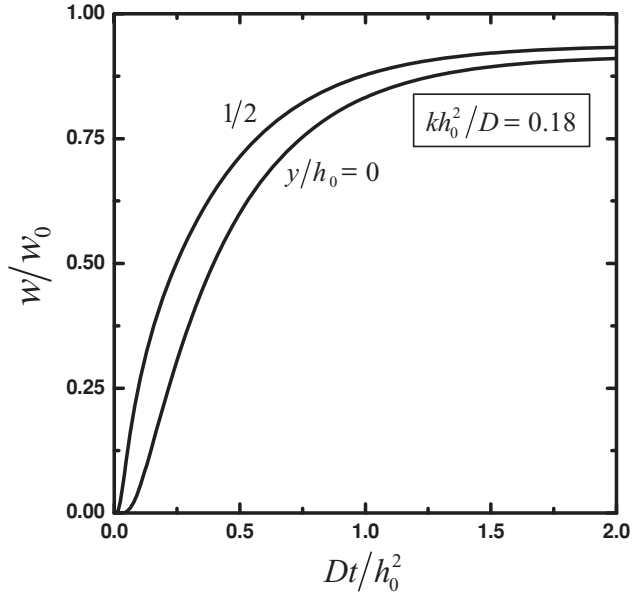

Figure 4. Water concentration versus time at the middle ($y/h_0 = 1/2$) and bottom ($y/h_0 = 0$) of the Mg layer.

of water that reacts at a given location (per unit volume), the mass of dissolved porous material (per unit volume) is $kwM/(qM_{H_2O})$, where M and M_{H_2O} are the molar masses of porous material and water, respectively. The net mass of porous material dissolved is obtained by integrating Equation (15) over both the thickness direction y and time t, where in turn gives a scaling law of the thickness h of the porous material layer normalized by its initial thickness h_0 before complete physical disappearance as

$$\frac{h}{h_0} = 1 - \frac{w_0 M}{q\rho M_{H_2O}}\frac{kh_0^2}{D}$$

$$\left\{\frac{Dt}{h_0^2}\cdot\frac{\tanh\sqrt{\frac{kh_0^2}{D}}}{\sqrt{\frac{kh_0^2}{D}}} - 2\sum_{n=1}^{\infty}\frac{1-e^{-\left[\frac{kh_0^2}{D}+\left(n-\frac{1}{2}\right)^2\pi^2\right]\frac{Dt}{h_0^2}}}{\left[\frac{kh_0^2}{D}+\left(n-\frac{1}{2}\right)^2\pi^2\right]^2}\right\} \tag{18}$$

where ρ is the mass density of porous material. It is clear that the normalized thickness, h/h_0, depends on the normalized time Dt/h_0^2, non-dimensional parameter kh_0^2/D, and is linear with a single combination of water concentration w_0 and mass density ρ of porous material, $w_0 M/(q\rho M_{H_2O})$.

For the parameters k and D in the present study, the summation on the right hand side of Equation (18) is negligible such that the thickness has a simple and approximate expression

$$h \approx h_0 - \frac{w_0 M}{q\rho M_{H_2O}}\sqrt{kD}\tanh\sqrt{\frac{kh_0^2}{D}}\cdot t \tag{19}$$

which decreases linearly with time t. This means that the steady-state solution in Equation (17) dominates the contribution to the water concentration in Equation (15). The normalized form of Equation (19) is

$$\frac{h}{h_0} \approx 1 - \frac{t}{t_c} \tag{20}$$

where

$$t_c = \frac{h_0}{\sqrt{kD}}\frac{q\rho M_{H_2O}}{w_0 M}\frac{1}{\tanh\sqrt{\frac{kh_0^2}{D}}} \tag{21}$$

is the critical time for the thickness to reach zero. For Mg (molar mass M = 24 g mol^{-1}, mass density ρ = 1.738 g cm^{-3}) with the initial thickness h_0 = 300 nm to react with water (molar mass M_{H_2O} = 18 g mol^{-1}, water concentration w_0 = 1 g cm^{-3}, and q = 2 water molecules reacting with 1 Mg atom), this critical time t_c is 38 min, which agrees reasonably well with experiments, to be discussed in **Figure 5**. Equation (20) shows that the thickness deceases linearly with time. Therefore, the rate of dissolution is

$$v_{\text{dissolution}} = -\frac{dh}{dt} \approx \frac{h_0}{t_c} = \sqrt{kD}\frac{w_0 M}{q\rho M_{H_2O}}\tanh\sqrt{\frac{kh_0^2}{D}} \tag{22}$$

As shown in **Table 1**, the rate of dissolution is 0.044, 0.13, and 0.20 nm s^{-1} (or equivalently 160, 470, and 710 nm h^{-1}) for 100, 300, and 500-nm-thick Mg layers, respectively. They are on the same order as the rate of dissolution reported in

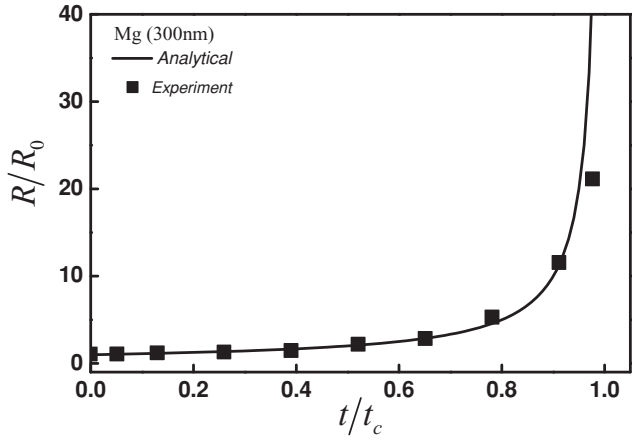

Figure 5. Experimental and analytical results of electric resistance of Mg (300 nm thick).

experiments, such as 0.069 nm s^{-1} in the citric acid-Na_2HPO_4 buffer system with PH 7.4[12] and 0.096 nm s^{-1} in conventional chloride solution.[13] However, the rate of dissolution depends strongly on the surrounding liquid, such as 0.48 nm s^{-1} in the 0.125 M NaCl,[14] 1.3–2.9 nm s^{-1} in the normal simulated body fluid (SBF),[15] and as high as 940 nm s^{-1} in 0.3 M $MgCl_2$.[16] Equation (21) and Equation (22) show the important scaling laws for all materials properties that come into play.

The electric resistance (per unit length) is inversely proportional to the thickness and is given by

$$R = R_0 \frac{h_0}{h} \approx \frac{R_0}{1-\frac{t}{t_c}} \tag{23}$$

where R_0 is the initial resistance (per unit length). For Mg with the initial thickness h_0 = 300 nm and initial resistance (per unit length) R_0 = 1.06 Ω mm^{-1} to react with water, Figure 5 shows the normalized electric resistance R/R_0 versus the normalized time t/t_c. The analytical result from Equation (23) agrees well with the experiments for the reaction constant k = 1.2×10^{-3} s^{-1} and diffusivity $D = 6.0 \times 10^{-12}$ cm^2 s^{-1}. The critical time t_c for complete dissolution of Mg is 38 min obtained from Equation (21), which agrees well with 40 min for open circuit in experiments. It should be pointed out that the dissolution of Mg may involve an initial layer of MgO on the surface, which will be quickly replaced by the more stable hydroxide in the presence of water.[17] This thin $Mg(OH)_2$ film on Mg is generally regarded as crystalline and is not as protective as non-crystalline films,[18] thereby suggesting that the single-layer dissolution model is applicable to Mg.

Table 1. Dissolution rate in water [nm h^{-1}].

Initial thickness [nm]	Mg	Mg/MgO (400 nm)	Mg/MgO (400 nm) + silk	Mg/MgO (800 nm)	Mg/MgO (800 nm) + silk
100	160	52	28	15	1.5
300	470	85	47	23	2.3
500	710	96	53	26	2.6

For dissolution of PECVD SiO_2 dielectric (molar mass M = 60 g mol^{-1}, mass density ρ = 2.648 g cm^{-3}) with the initial thickness h_0 = 35, 70, and 100 nm in water (molar mass $M_{H_2O} = 18$ g mol^{-1}, water concentration w_0 = 1 g cm^{-3}, and q = 2 water molecules reacting with 1 SiO_2 molecule), the diffusivity and reaction constant between water and PECVD SiO_2 dielectric are obtained from the experiments as $D = 1.0 \times 10^{-16}$ cm^2 s^{-1} and $k = 1.5 \times 10^{-6}$ s^{-1} at room temperature, and $D = 2.0 \times 10^{-16}$ cm^2 s^{-1} and $k = 3.0 \times 10^{-6}$ s^{-1} at body temperature. These values of D fall within the range of diffusivity reported in experiments,[19–26] which depends on the temperature. Here k for SiO_2 (~10^{-6} s^{-1}) is much smaller than that for Mg (~10^{-3} s^{-1}) because the water-Mg reaction is much faster (minutes to dissolve Mg versus days to dissolve SiO_2). The non-dimensional parameters are $w_0 M/(q\rho M_{H_2O}) = 0.63$ and $kh_0^2/D = 0.18$, 0.74 and 1.5 for three initial thicknesses and room temperature. **Figure 6** shows the normalized thickness h/h_0 of SiO_2 at room temperature versus normalized time Dt/h_0^2 as defined in Equation (16). The analytical results from Equation (18) agree well with experiments for all three initial thicknesses. The critical time to dissolve SiO_2 with initial thickness of 35, 70, and 100 nm is 13, 15, and 18 days, respectively, which agree reasonably well with experiments shown in Figure 6. The corresponding rates of dissolution are 0.11, 0.19, and 0.23 nm h^{-1} at room temperature, respectively, and they increase to 0.22, 0.39, and 0.47 nm h^{-1} at the body temperature. These rates for PECVD SiO_2 are consistent with the rates reported in prior experiments,[27,28] but are higher than those for quartz.[29,30]

3. Double-Layer Reactive Diffusion

The timeframe to dissolve a layer of Mg with the initial thickness h_0 is defined by the material itself, as given in Equation (21). Figure 2b shows an encapsulation layer of MgO with initial

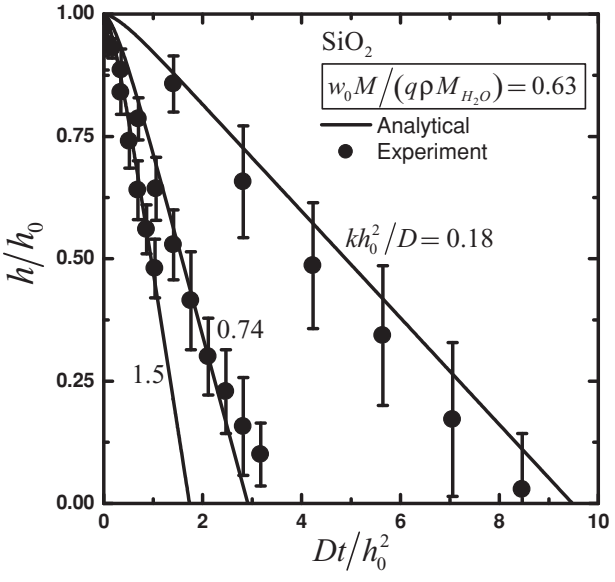

Figure 6. Experimental and analytical results of SiO_2 thickness (initial thickness 35, 70, and 100 nm).

thickness $h_{encapsulation}$ to provide another stage that the device functions stably. For the Mg layer, the reactive diffusion equation (1), zero water flux condition at the bottom surface $y = 0$ in Equation (2b), and zero initial condition at $t = 0$ in Equation (3) still hold. For the MgO encapsulation, the governing equation, boundary condition and initial condition are

$$D_{encapsulation}\frac{\partial^2 w}{\partial y^2} - k_{encapsulation}w = \frac{\partial w}{\partial t} \quad (h_0 \le y \le h_0 + h_{encapsulation})$$
$$w|_{y=h_0+h_{encapsulation}} = w_0$$
$$w|_{t=0} = 0 \quad (h_0 \le y \le h_0 + h_{encapsulation}) \tag{24a-c}$$

where $D_{encapsulation}$ and $k_{encapsulation}$ are the diffusivity of water and reaction constant between the encapsulation layer (e.g., MgO) and water, respectively. The constant water concentration condition in Equation (2a) is replaced by the continuity of concentration and flux of water molecules across the MgO/Mg interface, i.e.,

$$w|_{y=h_0-0} = w|_{y=h_0+0}$$
$$D\frac{\partial w}{\partial y}\bigg|_{y=h_0-0} = D_{encapsulation}\frac{\partial w}{\partial y}\bigg|_{y=h_0+0}. \tag{25a,b}$$

The water concentration w can be represented by a sum of the homogenous solution w_h and a particular solution w_p, i.e., $w = w_h + w_p$. Here the homogeneous solution w_h satisfies the following homogeneous boundary equations and boundary conditions

$$\begin{cases} D'\frac{\partial^2 w_h}{\partial y^2} - k'w_h = \frac{\partial w_h}{\partial t} \\ w_h|_{y=h_0+h_{encapsulation}} = 0 \\ \frac{\partial w_h}{\partial y}\Big|_{y=0} = 0 \end{cases} \tag{26a-c}$$

where $D' = D$ and $k' = k$ for $0 \le y \le h_0$, and $D' = D_{encapsulation}$ and $k' = k_{encapsulation}$ for $h_0 \le y \le h_0 + h_{encapsulation}$. The above equation can be solved by the method of separation variables, which gives the solution

$$w_h = \begin{cases} Ee^{-\lambda t}\cos\left(\sqrt{\frac{\lambda-k}{D}}y\right), 0 \le y \le h_0 \\ Fe^{-\lambda t}\sin\left[\sqrt{\frac{\lambda-k_{encapsulation}}{D_{encapsulation}}}\left(h_0 + h_{encapsulation} - y\right)\right], \\ h_0 \le y \le h_0 + h_{encapsulation} \end{cases} \tag{27a,b}$$

where E and F are constants to be determined. The continuity conditions in Equation (25) is applied to the homogeneous solution, which gives

$$\begin{bmatrix} \cos\left(\sqrt{\frac{\lambda-k}{D}}h_0\right) & -\sin\left(\sqrt{\frac{\lambda-k_{encapsulation}}{D_{encapsulation}}}h_{encapsulation}\right) \\ -\sqrt{(\lambda-k)\,D}\sin\left(\sqrt{\frac{\lambda-k}{D}}h_0\right) & \sqrt{(\lambda-k_{encapsulation})\,D_{encapsulation}}\cos\left(\sqrt{\frac{\lambda-k_{encapsulation}}{D_{encapsulation}}}h_{encapsulation}\right) \end{bmatrix} \begin{pmatrix} E \\ F \end{pmatrix} = 0 \tag{28}$$

The vanishing of its determinant, in order to have a non-trivial solution, leads to the following eigen equation

$$\tan\sqrt{\frac{\lambda-k}{D}h_0^2}\tan\sqrt{\frac{\lambda-k_{encapsulation}}{D_{encapsulation}}h_{encapsulation}^2} = \sqrt{\frac{(\lambda-k_{encapsulation})\,D_{encapsulation}}{(\lambda-k)\,D}} \tag{29}$$

from which a series of roots λ_n ($n = 1, 2, 3, \cdots$) can be determined. The homogeneous solution can then be obtained as

$$w_h = w_0\sum_{n=1}^{\infty} C_n e^{-\lambda_n t} f_n(y) \tag{30}$$

where the coefficients C_n, which replace E and F via Equation (28), are to be determined, and

$$f_n(y) \equiv \begin{cases} \sin\left(\sqrt{\frac{\lambda_n-k_{encapsulation}}{D_{encapsulation}}}h_{encapsulation}\right) \\ \cos\left(\sqrt{\frac{\lambda_n-k}{D}}y\right), \quad 0 \le y \le h_0 \\ \cos\left(\sqrt{\frac{\lambda_n-k}{D}}h_0\right)\sin \\ \left[\sqrt{\frac{\lambda_n-k_{encapsulation}}{D_{encapsulation}}}\left(h_0 + h_{encapsulation} - y\right)\right], \\ h_0 \le y \le h_0 + h_{encapsulation} \end{cases} \tag{31a,b}$$

The particular solution w_p, satisfying the Equations (1) and Equation (24a), non-homogeneous boundary conditions (2b) and (24b), and continuity conditions (25), is obtained as

$$w_p = w_0 g(y) \tag{32}$$

where

$$g(y) \equiv \begin{cases} G\cosh\left(\sqrt{\frac{k}{D}}y\right), \quad 0 \le y \le h_0 \\ \cosh\left(\xi\frac{h_0+h_{encapsulation}-y}{h_{encapsulation}}\right) \\ -H\sinh\left(\xi\frac{h_0+h_{encapsulation}-y}{h_{encapsulation}}\right), \\ h_0 \le y \le h_0 + h_{encapsulation} \end{cases} \tag{33a,b}$$

$$G = \frac{1}{\sqrt{\frac{Dk}{D_{encapsulation}k_{encapsulation}}}\sinh\sqrt{\frac{kh_0^2}{D}}\sinh\xi + \cosh\sqrt{\frac{kh_0^2}{D}}\cosh\xi}$$
$$H = \frac{\sqrt{\frac{Dk}{D_{encapsulation}k_{encapsulation}}}\tanh\sqrt{\frac{kh_0^2}{D}} + \tanh\xi}{\sqrt{\frac{Dk}{D_{encapsulation}k_{encapsulation}}}\tanh\sqrt{\frac{kh_0^2}{D}}\tanh\xi + 1} \tag{34a,b}$$

and $\xi = \sqrt{k_{encapsulation}h_{encapsulation}^2 / D_{encapsulation}}$. The water concentration w is the sum of w_h in Equation (30) and w_p in Equation (32),

$$w = w_0\left[\sum_{n=1}^{\infty} C_n e^{-\lambda_n t} f_n(y) + g(y)\right] \tag{35}$$

The initial conditions (3) and (20c) require

$$\sum_{n=1}^{\infty} C_n f_n(\gamma) + g(\gamma) = 0 \tag{36}$$

The orthogonality of eigenfunctions $\int_0^{h_0+h_{\text{encapsulation}}} f_m(\gamma) f_n(\gamma)\, d\gamma = 0$ (if $m \neq n$) gives analytically the coefficient C_n as

$$C_n = -\frac{\int_0^{h_0+h_{\text{encapsulation}}} f_n(\gamma) g(\gamma) d\gamma}{\int_0^{h_0+h_{\text{encapsulation}}} f_n^2(\gamma) d\gamma} = \frac{\left[-\frac{2}{\lambda_n}\sqrt{(\lambda_n - k_{\text{encapsulation}})\, D_{\text{encapsulation}}}\right]\left[\cos\left(\sqrt{\frac{\lambda_n - k}{D}} h_0\right)\right]}{\left\{h_0 \sin^2\left(\sqrt{\frac{\lambda_n - k_{\text{encapsulation}}}{D_{\text{encapsulation}}}} h_{\text{encapsulation}}\right)\left[1 + \frac{\sin\left(2\sqrt{\frac{\lambda_n - k}{D}} h_0\right)}{2\sqrt{\frac{\lambda_n - k}{D}} h_0}\right] + h_{\text{encapsulation}} \cos^2\left(\sqrt{\frac{\lambda_n - k}{D}} h_0\right)\left[1 - \frac{\sin\left(2\sqrt{\frac{\lambda_n - k_{\text{encapsulation}}}{D_{\text{encapsulation}}}} h_{\text{encapsulation}}\right)}{2\sqrt{\frac{\lambda_n - k_{\text{encapsulation}}}{D_{\text{encapsulation}}}} h_{\text{encapsulation}}}\right]\right\}} \tag{37}$$

Its substitution into Equation (35) gives the solution of the double-layer reactive diffusion equation. Besides depending on the normalized position γ/h_0, time Dt/h_0^2, and the non-dimensional parameters kh_0^2/D as in the single-layer solution in Section 2, the normalized water concentration w/w_0 also depends on the normalized reaction constant $k_{\text{encapsulation}}h_{\text{encapsulation}}^2 / D_{\text{encapsulation}}$ of the encapsulation, and the diffusivity ratio $D_{\text{encapsulation}}/D$ and initial thickness ratio $h_{\text{encapsulation}}/h_0$. **Figure 7** shows the distribution of water concentration in both layers (w/w_0 versus γ/h_0) for Dt/h_0^2 = 1.2, 2.4, 4.8, 12, ∞, and the non-dimensional parameters $kh_0^2/D = 0.18$, $k_{\text{encapsulation}}h_{\text{encapsulation}}^2 / D_{\text{encapsulation}} = 1.6$, $D_{\text{encapsulation}}/D = 0.082$, and $h_{\text{encapsulation}}/h_0 = 1.3$, which correspond to $k = 1.2 \times 10^{-3}$ s^{-1}, $D = 6.0 \times 10^{-12}$ cm^2 s^{-1} and h_0 = 300 nm of Mg (the same as those in Section 2), and $k_{\text{encapsulation}} = 5.0 \times 10^{-4}$ s^{-1}, $D_{\text{encapsulation}} = 4.9 \times 10^{-13}$ cm^2 s^{-1} and $h_{\text{encapsulation}}$ = 400 nm of MgO in the experiment. The above diffusivity $D_{\text{encapsulation}}$ falls within the range ($3.2 \times 10^{-13} \sim 7.9 \times 10^{-13}$ cm^2 s^{-1}) reported in the experiment for MgO,[31] but is different from the other experiments because of very different temperatures and environments (e.g., Eastman and Cutler[32] for an isolated water molecule into (001) MgO, McCarthy et al.[33] for diffusion of O_2 into MgO, Leeuw and Parker[34] for self diffusion of MgO). The reaction constant of MgO, $k_{\text{encapsulation}} = 5.0 \times 10^{-4}$ s^{-1}, is consistent with that extracted from the prior experiments for a single layer MgO.[35–38] For 100-nm-thick MgO layer, Equation (22) gives the rate of dissolution 0.010 nm s^{-1}, which falls within the range of ≈10^{-4}–0.01 nm s^{-1} reported in the experiments. The distribution of water concentration in Mg is quite uniform whereas that in MgO is non-uniform because the diffusion of water in Mg is much faster than that in MgO (e.g., $D_{\text{encapsulation}}/D = 0.082$). As compared to Figure 3 for a single layer, the water concentration in Mg increases slowly because of the encapsulation layer.

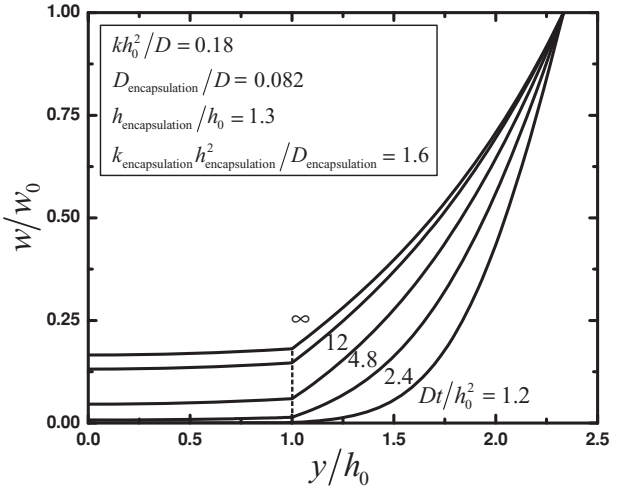

Figure 7. Distribution of water concentration in both Mg and MgO layers.

In the same manner as described in Section 2, the thickness h of the Mg layer normalized by its initial thickness h_0 before complete physical disappearance is obtained as

$$\frac{h}{h_0} = 1 - \frac{w_0 M}{q\rho M_{H_2O}} k \left[Gt \cdot \frac{\sinh\sqrt{\frac{kh_0^2}{D}}}{\sqrt{\frac{kh_0^2}{D}}} + \sum_{n=1}^{\infty} \frac{C_n}{\lambda_n}\left(1 - e^{-\lambda_n t}\right) \frac{\sin\sqrt{\frac{\lambda_n - k}{D}} h_0^2}{\sqrt{\frac{\lambda_n - k}{D}} h_0^2} \sin\sqrt{\frac{\lambda_n - k_{\text{encapsulation}}}{D_{\text{encapsulation}}}} h_{\text{encapsulation}}^2 \right] \tag{38}$$

where q = 2, molar mass M = 24 g mol^{-1} and mass density ρ = 1.738 g cm^{-3} for Mg, and G is given in Equation (34a). The electric resistance (per unit length) of this double-layer structure is inversely proportional to the thickness of Mg layer because MgO is not a conductor. The electric resistance is given analytically by

$$R = R_0 \frac{h_0}{h} \tag{39}$$

For a 300-nm-thick Mg layer with the 400-nm-thick MgO encapsulation layer, the measured initial resistance (per unit length) is 1.04 Ω mm^{-1}. Another 300-nm-thick Mg layer, which has different width and length and an 800 nm-thick encapsulation layer, has an initial resistance of 1.15 Ω mm^{-1}. **Figure 8** shows the normalized electric resistance R/R_0 versus the normalized time Dt/h_0^2 for the single-layered Mg, and Mg with 400- and 800-nm-thick MgO encapsulation layers. The thickness of Mg layer is fixed at 300 nm. The analytical results from Equation (38) and Equation (39) agree well with the experiments. The dissolution time increases substantially with the thickness of encapsulation layer, which provides an effective way to control the dissolution time.

In order to further extend the dissolution time a silk overcoat is used to provide a barrier for water to diffuse into MgO

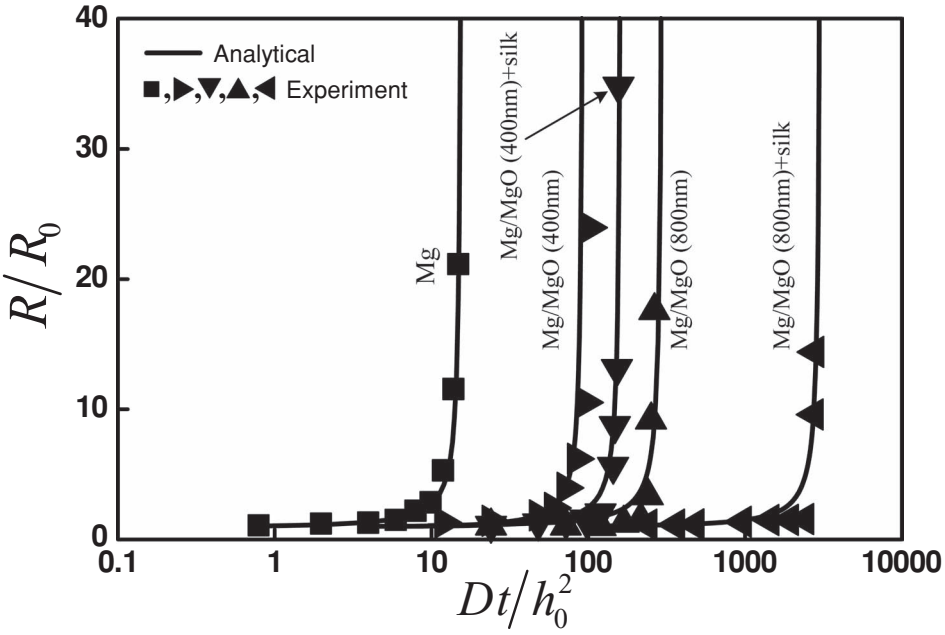

Figure 8. Experimental and analytical results of electric resistance for Mg, Mg with MgO encapsulation layers and two different silk overcoats with φ = 45% and 90%, respectively.

and Mg layers. The effective diffusion is controlled by the percentage φ of the maximum crystallinity c_{max} that can be achieved in the silk,[39,40] which gives the crystallinity of silk $c = \varphi c_{max}$. The boundary condition of the constant water concentration at water/MgO interface in Equation (24b) is then replaced by $w|_{y=h_0+h_{encapsulation}} = (1-\phi)\, w_0$. The corresponding solutions are readily obtained by replacing w_0 with $(1-\varphi)w_0$ in this section. For example, the water concentration in Equation (35) becomes

$$w = (1-\phi)\, w_0 \left[\sum_{n=1}^{\infty} C_n e^{-\lambda_n t} f_n(y) + g(y) \right] \tag{40}$$

where C_n, λ_n, f_n and g are still given by Equation (37), Equation (29), Equation (31) and Equation (33), respectively. The electric resistance in Equation (39) also holds, but w_0 in Equation (38) for the thickness is replaced with $(1-\varphi)w_0$. Figure 8 shows the electric resistance for Mg with MgO encapsulation layers and two different silk overcoats with φ = 45% and 90%, respectively. Results for a single layer of Mg (Figure 5) are also shown in Figure 8 for comparison. For Mg with 400 nm-thick MgO encapsulation layer and silk overcoat with φ = 45%, the dissolution time is about 1.5 times larger than that without the overcoat. For Mg with 800-nm-thick MgO encapsulation layer and silk overcoat with φ = 90%, the dissolution time increases substantially to more than 10 times of that without the overcoat. The dissolution time increases with the crystallinity (φc_{max}) because a higher crystallinity provides a stronger barrier for the water to diffuse into MgO and Mg. The analytical results in Figure 8 all agree well with experiments.

The summation on the right hand side of Equation (38) and Equation (40) is negligible for the parameters in the present study such that the thickness decreases linearly with time, and has a simple and approximate expression

$$\frac{h}{h_0} \approx 1 - \frac{t}{t_c'} \tag{41}$$

where

$$t_c' = \frac{t_c}{(1-\phi)\, G \cosh\sqrt{\frac{kh_0^2}{D}}} = \frac{t_c}{1-\phi} \left(\sqrt{\frac{k\,D}{k_{encapsulation}\, D_{encapsulation}}} \tanh\sqrt{\frac{kh_0^2}{D}} \sinh\xi + \cosh\xi \right) \tag{42}$$

is the critical time for the Mg layer to reach zero, and t_c is the critical time without the encapsulation given in Equation (21). Equation (42) gives 3.5 and 13 h for the 400-nm- and 800-nm-thick MgO encapsulation layers without the silk overcoat, respectively. With the overcoat they increase to 6.4 and 130 h, respectively. These dissolution times agree well with the time for open circuit in experiments.

Equation (41) gives the rate of dissolution

$$v_{dissolution} = -\frac{dh}{dt} \approx \frac{h_0}{t_c'} = \frac{(1-\phi)\sqrt{k\,D}\,\frac{w_0 M}{q\rho M_{H_2O}}}{\sqrt{\frac{k\,D}{k_{encapsulation}\, D_{encapsulation}}} \sinh\xi + \coth\sqrt{\frac{kh_0^2}{D}} \cosh\xi} \tag{43}$$

Table 1 shows the dissolution rate for Mg, Mg/MgO, and Mg/MgO+silk. The initial thickness of Mg layer is 100, 300 and 500 nm. The dissolution rate depends strongly on the materials, ranging from ≈1 nm min^{-1} for Mg to ≈1 nm h^{-1} for Mg/MgO (800 nm)+silk. For each material, the dissolution rate is approximately linear with the initial thickness h_0 for sufficiently thin Mg layer, and is given by

$$v_{\text{dissolution}} = (1-\phi)\frac{\omega_0 M}{q\rho M_{H_2O}}\frac{kh_0}{\cosh\xi} \text{ for } kh_0^2/D \ll 1. \quad (44)$$

The dissolution rate increases with the initial thickness h_0. For relatively large h_0, it saturates at

$$v_{\text{dissolution}} = (1-\phi)\frac{\sqrt{kD}\frac{\omega_0 M}{q\rho M_{H_2O}}}{\sqrt{\frac{kD}{k_{\text{encapsulation}} D_{\text{encapsulation}}}}\sinh\xi + \cosh\xi} \text{ for } kh_0^2/D \gg 1 \quad (45)$$

4. Concluding Remarks and Discussion

Analytical models for the transient electronic systems have been established. For single- and double-layered structures (with or without the silk overcoat) in solution, the remaining height and electric resistance of the system are obtained analytically. In particular, the dissolution time and rate of dissolution are given analytically in terms of the reaction constant and diffusivity of each material in the solution, molar masses and mass density of materials and solution, solution concentration, number of solution molecules reacting with each atom, crystallinity of silk overcoat, and thickness of each layer. The analytical models agree well with the experiments for Mg single layer, Mg/MgO double layer (with and without overcoat), and are useful for design of transient electronic components.

The model of reactive diffusion can also be applied at the system level. To demonstrate this capability, in vivo transience of an implantable RF metamaterial antenna is tested. The quality factor or Q factor[41] measured in experiments, which describes how under-damped a resonator is, or equivalently, characterizes a resonator's bandwidth relative to its center frequency, also agrees well with the analytical models.[1]

It should be pointed out that the range of reaction constant reported in the literature is very large because it depends on many factors that can vary vastly in experiments, such as morphologies of the materials, temperature, and the PH value, concentration, and properties (e.g., ion concentration) of the surrounding liquid. The reaction constants and diffusivities reported in this paper for Mg, MgO, and SiO_2 are close to, or on the same order as, those reported in the literature under similar conditions. However, any of these constants can be extremely sensitive to the conditions so that those provided in this paper do not have to be universal.

Acknowledgements

R.L., H.C., and Y.S. contributed equally to this work. The authors acknowledge support from NSF-INSPIRE (1242240).

Received: October 22, 2012
Revised: December 16, 2012
Published online: January 21, 2013

[1] S.-W. Hwang, H. Tao, D.-H. Kim, H. Cheng, J.-K. Song, E. Rill, M. A. Brenckle, B. Panilaitis, S. M. Won, Y.-S. Kim, Y. M. Song, K. J. Yu, A. Ameen, R. Li, Y. Su, M. Yang, D. L. Kaplan, M. R. Zakin, M. J. Slepian, Y. Huang, F. G. Omenetto, J. A. Rogers, *Science* **2012**, *337*, 1640.
[2] C. J. Bettinger, Z. Bao, *Adv. Mater.* **2010**, *22*, 651.
[3] M. Irimia-Vladu, P. A. Troshin, M. Reisinger, L. Shmygleva, Y. Kanbur, G. Schwabegger, M. Bodea, R. Schwodiauer, A. Mumyatov, J. W. Fergus, V. F. Razumov, H. Sitter, N. S. Sariciftci, S. Bauer, *Adv. Funct. Mater.* **2010**, *20*, 4069.
[4] C. Legnani, C. Vilani, V. L. Calil, H. S. Barud, W. G. Quirino, C. A. Achete, S. J. L Ribeiro, M. Cremona, *Thin Solid Films* **2008**, *517*, 1016.
[5] D. H. Kim, J. Viventi, J. J. Amsden, J. L. Xiao, L. Vigeland, Y. S. Kim, J. A. Blanco, B. Panilaitis, E. S. Frechette, D. Contreras, D. L. Kaplan, F. G. Omenetto, Y. G. Huang, K. C. Hwang, M. R. Zakin, B. Litt, J. A. Rogers, *Nat. Mater.* **2010**, *9*, 511.
[6] H. Seidel, L. Csepregi, A. Heuberger, H. Baumgärtel, *J. Electrochem. Soc.* **1990**, *137*, 3612.
[7] D. H. Davies, G. T. Burstein, *Corrosion* **1980**, *36*, 416.
[8] V. Fournier, P. Marcus, I. Olefjord, *Surf. Interface Anal.* **2002**, *34*, 494.
[9] M. J. Spearpoint, J. G. Quintiere, *Combust. Flame* **2000**, *123*, 308.
[10] P. V. Danckwerts, *Trans. Faraday Soc.* **1950**, *46*, 300.
[11] I. A. Taub, W. Roberts, S. LaGambina, K. Kustin, *J. Phys. Chem. A* **2002**, *106*, 8070.
[12] W. F. Ng, K. Y. Chiu, F. T. Cheng, *Mater. Sci. Eng. C* **2010**, *30*, 898.
[13] H. Inoue, K. Sugahara, A. Yamamoto, H. Tsubakino, *Corros. Sci.* **2002**, *44*, 603.
[14] A. Yamamoto, S. Hiromoto, *Mater. Sci. Eng. C* **2009**, *29*, 1559.
[15] G. Song, S. Song, *Adv. Eng. Mater.* **2007**, *9*, 298.
[16] E. J. Casey, R. E. Bergeron, G. D. Nagy, *Can. J. Chem.* **1962**, *40*, 463.
[17] M. Pourbaix, *Atlas of electrochemical equilibria in aqueous solutions*, National Association of Corrosion Engineers, Houston **1974**.
[18] T. P. Hoar, *J. Electrochem. Soc.* **1970**, *117*, 17C.
[19] R.K. Iler, *J. Colloid Interface Sci.* **1973**, *43*, 399.
[20] M. Nogami, M. Tomozawa, *J. Am. Ceram. Soc.* **1984**, *67*, 151.
[21] H. Wakabayashi, M. Tomozawa, *J. Am. Ceram. Soc.* **1989**, *72*, 1850.
[22] K. Fukuda, T. Nakano, M. Fujishima, N. Mura, K. Tokunaga, S. Ichinose, *Jap. J. Appl. Phys.* **1994**, *33*, L1445.
[23] S. Ulutan, D. Balköse, *J. Membr. Sci.* **1996**, *115*, 217.
[24] R. H. Doremus, *Earth Planet. Sci. Lett.* **1998**, *163*, 43.
[25] M. Tomozawa, K. M. Davis, *Mat. Sci. Eng.* **1999**, *A272*, 114.
[26] J. Thurn, *J. Non-Cryst. Solids* **2008**, *354*, 5459.
[27] D. C. Hurd, F. Theyer, *Adv. Chem. Ser.* **1975**, *147*, 211.
[28] G. S. Wirth, J. M. Gieskes, *J. Colloid Interface Sci.* **1979**, *68*, 492.
[29] K. G. Knauss, T. J. Wolery, *Geochim. Cosmochim. Acta* **1988**, *52*, 43.
[30] W. G. Worley, *Dissolution kinetics and mechanisms in quartz- and grainite-water systems,* Ph. D. thesis, Massachusetts Institute of Technology, **1994.**
[31] B. Joachim, E. Gardés, R. Abart, W. Heinrich, *Contrib. Mineral. Petrol.* **2011**, *161*, 389.
[32] P. F. Eastman, I. B. Cutler, *J. Am. Chem. Soc.* **1966**, *49*, 526.
[33] M. I. McCarthy, G. K. Schenter, C. A. Scamehorn, J. B. Nicholas, *J. Phys. Chem.* **1996**, *100*, 16989.
[34] N. H. de Leeuw, S. C. Parker, *Phys. Rev. B* **1998**, *58*, 13901.
[35] D. D. Macdonald, D. Owen, *Can. J. Chem.* **1971**, *49*, 3375.
[36] K. Sangwal, *J. Mater.Sci.* **1982**, *17*, 3598.
[37] O. Fruhwirth, G. W. Herzog, I. Hollerer, A. Rachetti, *Surf. Technol.* **1985**, *24*, 301.
[38] J. A. Mejias, A. J. Berry, K. Refson, D. G. Fraser, *Chem. Phys. Lett.* **1999**, *314*, 558.
[39] L. Segal, J. J. Creely, A. E. Martin Jr., C. M. Conrad, *Text. Res. J.* **1959**, *29*, 786.
[40] W. Ruland, *Acta Crystallogr.* **1961**, *14*, 1180.
[41] M. Rodahl, F. Hook, A. Krozer, P. Brzezinski, B. Kasemo, *Rev. Sci. Instrum.* **1995**, *66*, 3924.